DINAME 2017 - Proceedings of the XVII International Symposium on Dynamic Problems of Mechanics
A. T. Fleury, D. A. Rade, P. R. G. Kurka (Editors), ABCM, São Sebastião, SP, Brazil, March 5-10, 2017

STRUCTURAL NONLINEARITIES EFFECT ON AEROELASTIC BIFURCATION PHENOMENA IN AIRFOILS

Daniel A. Pereira[a], **Carlos R. dos Santos**[b] **and Flávio D. Marques**[b]

[a] Mechanical Engineering, Aeronautics Institute of Technology, São José dos Campos, SP, Brazil
[b] Engineering School of São Carlos, University of São Paulo, Brazil

Abstract: Nonlinear aeroelastic behavior can be originated from aerodynamic and/or structural dynamics, therefore leading to several problems such as instabilities, limit cycle oscillations, bifurcations, and chaotic behavior. The objective of this work is to analyze and identify the dynamic response of a typical aeroelastic with structural hardening and free-play nonlinearities acting simultaneously. The effect of hardening corresponds to a smooth nonlinear increasing in restoring structural loading for a given displacement. This effect is modeled here by means of rational polynomial function, while the free-play is represented by hyperbolic functions combination. Aeroelastic responses are analyzed from computational and experimental results. The numerical model is based on the classical theory for the linear unsteady aerodynamics with corrections for arbitrary motions coupled to typical aeroelastic section model. Hopf bifurcations are identified and diagrams of amplitudes versus airspeeds are used to investigate the conditions in which the system is supercritical or subcritical. Higher-order spectra analysis is also used to check on frequency couplings, thereby allowing the identification of quadratic- and cubic-like nonlinear behavior. The study of the phenomena associated with the hardening, free-play and their intensity variation effects provide ways to mitigate or circumvent any undesired responses to those behaviors. This contributes to determining safety margins for aircraft even with these nonlinearities, as fully linear systems represent major challenges to achieving, and results in very high costs.

Keywords: Aeroelasticity, subcritical bifurcation, hardening, free-play, higher-order spectra analysis.

INTRODUCTION

The aeroelasticity is a multidisciplinary field of the aerospace engineering that deals with the mutual interaction between structural dynamics and non-stationary aerodynamic flow (Bisphinghoff *et al.*, 1996). Aeroelastic systems may behave nonlinearly, therefore subject to behavior such as bifurcations, limit cycle oscillations (LCO), and chaos (Sheta *et al.*, 2002). These phenomena, whose origins are both from structural dynamics and/or from the unsteady aerodynamic loading, may be difficult to predict. The concentrated structural nonlinear effects can be incorporated into numerical models through the elastic restoring forces or moments representations. The most common types of concentrated nonlinearities representations can be given by polynomial functions, nonlinear damping effects, free-play, hysteresis, etc.

The literature is vast and many authors have been studying nonlinear aeroelastic problems in the aviation, for example, the limit cycle oscillations have caused persistent problems in many aircraft designs, such as the F-16, where Chen *et al.* (1998) have observed the existence of hardening nonlinearity in wings pitching moment stiffness. O'Neil and Strgnac (1998) have developed an experimental model that provides direct measurements from the typical aeroelastic section with cubic nonlinearity in the pitch and plunge motion where they examined the sensitivity of the response to system parameters. Recently, Vasconcellos *et al.* (2012) have shown that the hyperbolic tangent function combination approach for modeling discontinuous nonlinearities is appropriate for detecting different nonlinear behaviors, including the experimentally observed LCO, chaos and transitions.

It is known that the system behavior is directly related to the nonlinearities involved, for example, system under free-play shows subcritical behavior. The Figure 1(a) and 1(b) represent the classical bifurcation diagram for the supercritical and subcritical behavior respectively where the limit cycle amplitude is plotted versus some system parameter, for example, the flight speed. In general, if the system depends on the initial condition and has different solution when the airspeed velocity is increased and decreased near the nonlinear critical velocity, the bifurcation is called subcritical, i.e. the LCOs may also exist below the flutter boundary (unstable LCO, dashed line). However, if the system are independent of the initial condition and the system stability changes only after the critical flutter velocity, the bifurcation is called supercritical and the system has only stable LCO (solid line) which sometimes is welcome because without it the LCO would instead be replaced by catastrophic flutter leading to loss of the flight vehicle (Dowell *et al.*, 2002). Bifurcation analysis is used to indicate quantitative and qualitative changes in the features of system, such as the number and type of solutions, under the variation of one or more parameters on which the considered system depends (Nayfeh and Balachandran, 1995).

This paper presents an investigation on the influence in bifurcation behavior of typical nonlinear aeroelastic section due to combined hardening and free-play effects. Numerical and experimental results are presented, thereby allowing

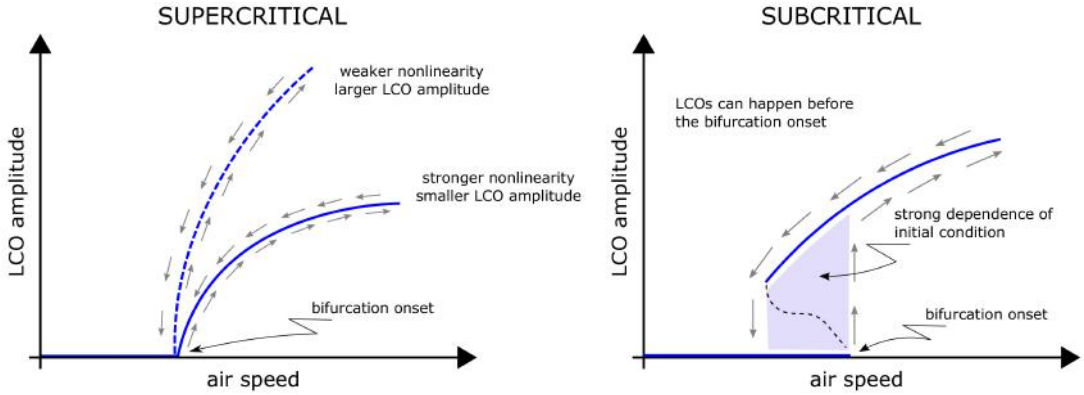

Figure 1 – Supercritical bifurcation diagram leading to only stable LCO (solid line) and subcritical bifurcation diagram leading to both stable and unstable LCO (dashed line).

comparisons and conclusions of the nonlinear features. Hardening nonlinearities with varying intensities in airfoil pitching motion and free-play (different gap values) in the control surface hinge were considered. Numerical model includes classical linear unsteady aerodynamics, while the equations of motion incorporate nonlinearities in the respective stiffness values. Traditional time integration method is used to aeroelastic simulations. The experimental apparatus was design to allow two-dimensional typical section behavior in plunge, pitch and control surface motions, and the test were performed using an open-circuit, blower-type low-speed wind tunnel. Bifurcation analysis comparing both numerical and experimental results was carried out, including a higher-order spectral (HOS) analysis to investigate on quadratic and cubic forms of nonlinear couplings due to the combined hardening and free-play effects.

METHODOLOGY

Numerical model for typical section

The mathematical model for typical section with three degrees of freedom and semi-chord b (*cf.* Figure 2) is derived from Bisphinghoff *et al.* (1996) and Theodorsen (1935), that is,

$$\begin{bmatrix} \mu_e & x_\alpha & x_\beta \\ x_\alpha & r_\alpha^2 & [r_\beta^2+(c-a)x_\beta] \\ x_\beta & [r_\beta^2+(c-a)x_\beta] & r_\beta^2 \end{bmatrix} \begin{Bmatrix} \ddot{\xi}(t) \\ \ddot{\alpha}(t) \\ \ddot{\beta}(t) \end{Bmatrix} + \begin{bmatrix} d_{1,1} & d_{1,2} & d_{1,3} \\ d_{2,1} & d_{2,2} & d_{2,3} \\ d_{3,1} & d_{3,2} & d_{3,3} \end{bmatrix} \begin{Bmatrix} \dot{\xi}(t) \\ \dot{\alpha}(t) \\ \dot{\beta}(t) \end{Bmatrix} + \begin{bmatrix} \omega_h^2 & 0 & 0 \\ 0 & r_\alpha^2\omega_\alpha^2 \frac{F(\alpha)}{\alpha(t)} & 0 \\ 0 & 0 & r_\beta^2\omega_\beta^2 \frac{F(\beta)}{\beta(t)} \end{bmatrix} \begin{Bmatrix} \xi(t) \\ \alpha(t) \\ \beta(t) \end{Bmatrix} = \begin{Bmatrix} -L(t)/(m_W b) \\ M_\alpha(t)/(m_W b^2) \\ M_\beta(t)/(m_W b^2) \end{Bmatrix}, \quad (1)$$

where the plunge, pitch and control surface displacements are given by h, α, and β, respectively, a and c are the dimensionless distances from the elastic axis to the middle and to the surface control, U is the airspeed, x_α and x_β are the dimensionless distances from elastic axis to wing center of gravity (CG) and the distance between the control surface and its CG, respectively, k_h, k_α, and k_β are the plunge, pitch and control surface stiffness, respectively, $\xi(t) = \frac{h(t)}{b}$, $\mu_e = \frac{m_T}{m_W}$, $d_{i,j}$ are the damping factors with respect to each airfoil motion and their influences (Rayleigh approach), $L(t)$ is the lift force, $M_\alpha(t)$ and $M_\beta(t)$ are the aerodynamic pitch and hinge moments, respectively, $F(\alpha)$ and $F(\beta)$ are functions related to nonlinearities applied to the stiffness.

$$L(t) = L^C + L^{NC}; \quad M_\alpha(t) = M_\alpha^C + M_\alpha^{NC}; \quad M_\beta(t) = M_\beta^C + M_\beta^{NC}, \quad (2)$$

where the circulatory terms (superscripts C) are:

$$L^C = 2\pi\rho U b C(k) f(t); \quad M_\alpha^C = 2\pi\rho b^2 (a+\tfrac{1}{2}) C(k) f(t); \quad M_\beta^C = -\rho U b^2 T_{12} C(k) f(t), \quad (3)$$

where $C(k)$ is the so-called Theodorsen function, and:

$$f(t) = U\alpha + \dot{h} + \dot{\alpha} b \left(\tfrac{1}{2} - a\right) + \tfrac{U}{\pi} T_{10}\beta + \tfrac{b}{2\pi} T_{11}\dot{\beta}\,, \quad (4)$$

is the quasi-steady term. The T-functions (T_i, for $i = 1, 2, \ldots$) are as defined in Theodorsen (1935). The non-circulatory terms (superscripts NC) are:

$$L^{NC} = \pi\rho b^2 \left[\ddot{h} + U\dot{\alpha} - ba\ddot{\alpha} - \frac{U}{\pi}T_4\dot{\beta} - \frac{b}{\pi}T_1\ddot{\beta}\right]; \tag{5}$$

$$M_\alpha^{NC} = \pi\rho b^2 \left\{ba\ddot{h} - Ub\left(\tfrac{1}{2} - a\right)\dot{\alpha} - b^2\left(\tfrac{1}{8} + a^2\right)\ddot{\alpha} - \frac{U^2}{\pi}(T_4 + T_{10})\beta + \right.$$
$$\left. \frac{Ub}{\pi}\left[-T_1 + T_8 + (c-a)T_4 - \tfrac{1}{2}T_{11}\right]\dot{\beta} + \frac{b^2}{\pi}[T_7 + (c-a)T_1]\ddot{\beta}\right\}; \tag{6}$$

$$M_\beta^{NC} = \pi\rho b^2 \left\{\frac{b}{\pi}T_1\ddot{h} + \frac{Ub}{\pi}\left[2T_9 + T_1 - \left(a - \tfrac{1}{2}\right)T_4\right]\dot{\alpha} - \frac{2b^2}{\pi}T_{13}\ddot{\alpha} - \frac{U^2}{\pi^2}(T_5 - T_4T_{10})\beta + \frac{UbT_4T_{11}}{2\pi^2}\dot{\beta} + \frac{b^2T_3}{\pi^2}\ddot{\beta}\right\}; \tag{7}$$

The aerodynamic loading, as given in Eq. (2), depend on the Theodorsen function $C(k)$, where $k = \omega b/U$ is the reduced frequency of harmonic oscillations. However, to account for arbitrary motions, an alternative is to manipulate the Theodorsen function by convolution based on Duhamel formulation in the time domain (Li *et al.*, 2010). If the Wagner function is also considered, it implies that, for instance, circulatory lift term can be written as:

$$C(k)f(t) = f(0)\phi(\tau) + \int_0^\tau \frac{f(\sigma)}{\sigma}\phi(\tau - \sigma)\mathrm{d}\sigma\,, \tag{8}$$

where σ is a dummy integration variable, and $\phi(\tau)$ is the Wagner function in the non-dimensional time $\tau = tU/b$, approximated by Sear's approach (Sears, 1940):

$$\phi(\tau) \approx c_0 - c_1 e^{-c_2\tau} - c_3 e^{-c_4\tau}, \tag{9}$$

where $c_0 = 1.0$, $c_1 = 0.165$, $c_2 = 0.0455$, $c_3 = 0.335$ and $c_4 = 0.3$.

Using integration by parts and following the state space method proposed by Lee *et al.* (2005), and Li *et al.* (2010), Eq. (8) leads to a circulatory term as:

$$C(k)f(t) = (c_0 - c_1 - c_3)f(t) + c_2c_4(c_1 + c_3)x_a + (c_1c_2 + c_3c_4)\dot{x}_a, \tag{10}$$

where x_a and $\dot{x}_a$ are augmented aerodynamic states. Substituting Eq. (10) in Eq. (3), one obtains the circulatory aerodynamic loads for the three degrees-of-freedom.

Given the previous arguments, the equations of motion for the aeroelastic system can be presented in the following final form:

$$(\mathbf{M}_s - \mathbf{M}_{nc})\ddot{\mathbf{x}} + (\mathbf{C}_s - \mathbf{C}_{nc} - \tfrac{1}{2}\mathbf{R}\mathbf{S}_2)\dot{\mathbf{x}} + (\mathbf{K}_s - \mathbf{K}_{nc} - \tfrac{1}{2}\mathbf{R}\mathbf{S}_1)\mathbf{x} - \mathbf{R}\mathbf{S}_3\mathbf{x}_a = \mathbf{0}; \tag{11}$$

$$\dot{\mathbf{x}}_a - \mathbf{E}_1\mathbf{x} - \mathbf{E_2}\dot{\mathbf{x}} - \mathbf{F}\mathbf{x}_a = \mathbf{0}, \tag{12}$$

where $\mathbf{x} = [\ \xi \quad \alpha \quad \beta\ ]^{\mathrm{T}}$ is the vector of structural generalized degrees of freedom, and $\mathbf{x}_a = [\ x_a \quad \dot{x}_a\ ]^{\mathrm{T}}$ is the vector of augmented aerodynamic states. Expressions for the matrices appearing in Eqs. (11) – (12) can be found in Vasconcellos *et al.* (2014). $\mathbf{M}_s$, $\mathbf{C}_s$, and $\mathbf{K}_s$ are the structural mass, damping and stiffness matrices, respectively; $\mathbf{M}_{nc}$, $\mathbf{C}_{nc}$, and $\mathbf{K}_{nc}$ are the non-circulatory flow contributions to mass, damping and stiffness matrices of the system, respectively; and $\mathbf{R}$, $\mathbf{S}_1$, $\mathbf{S}_2$, $\mathbf{S}_3$, $\mathbf{E}_1$, $\mathbf{E_2}$, and $\mathbf{F}$ are matrices and vectors that arise from the circulatory flow formulation, and that modify damping and stiffness properties, and couple the structural response with the time evolution of the augmented aerodynamic states.

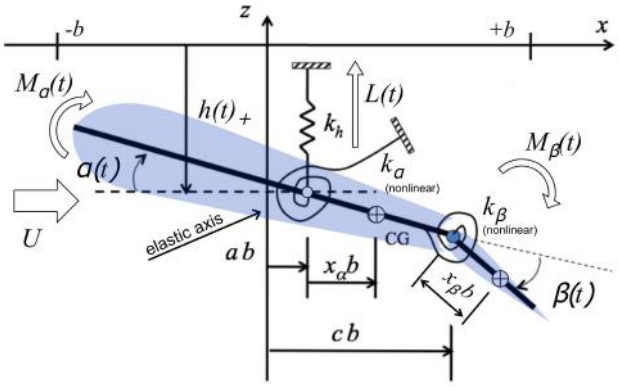

Figure 2 – Typical aeroelastic section.

Nonlinearities Representation

Functions $F(\alpha)$ and $F(\beta)$ in Eq. (1) are used to feed that aeroelastic set with the respective terms to account for nonlinearities in pitch and control surface responses. Here the hardening and free-play effects are combined for that motions (*cf.* Figure 3), being: *(i)* for pitching motion only hardening nonlinearity is considered, while, *(ii)* free-play is only affecting the control surface motion.

The hardening nonlinearity function in pitching ($F(\alpha)$) has been obtained using the rational polynomials (RP) approximation (Li *et al.*, 2012) from the experimentally measured restoring pitching moment curve (*cf.* Figure 3(a)). The RP approximation approach leads to the following ratio of polynomials form,

$$F(\alpha) = \frac{a_3\alpha^3 + a_2\alpha^2 + a_1\alpha + a_0}{b_2\alpha^2 + b_1\alpha + b_0} \quad , \tag{13}$$

where a_0 to a_3, and b_0 to b_2 are real-valued coefficients obtained numerically from measured experimental data.

For the free-play nonlinearity representation in the restoring torque of control surface, hyperbolic tangent functions combination is used the as proposed and validated by Vasconcellos *et al.* (2014). This function is given by:

$$F(\beta) = \frac{1}{2}[1 - \tanh(\varepsilon(\beta + \delta))]\,(\beta + \delta) + \frac{1}{2}[1 + \tanh(\varepsilon(\beta - \delta))]\,(\beta - \delta), \tag{14}$$

where δ denotes the lower and the upper freeplay boundaries, and ε is a variable which affects the smoothness of the function, where the higher is ε the free-play discontinuity is better represented. (*cf.* Fig. 3(b).)

Higher-Order Spectra

Higher-order spectra (HOS) moments are Fourier transforms of higher-order correlation functions with which it is possible to access more information on frequencies coupling. This Section presents the basic theoretical aspects of HOS analysis based on Nayfeh and Balachandran (1995) and Hajj and Beran (2008) . The Fourier or frequency spectra is an important tool that can help to identify and differentiate features of nonlinear systems related to stationary signals such as limit cycle oscillations and chaotic motions. Using Fourier transform the amplitude spectrum of a signal *x(t)* is,

$$X(f) = \int_0^T x(t)e^{-2i\pi ft}dt \quad . \tag{15}$$

where f denotes the frequency, $X(f)$ is a complex quantity and $x(t)$ is known for only a finite length of time *T*.

In order to get a measure of how random signals is correlated with itself, one can use the second order correlation (R_{xx}) for different period of time, which is given by,

$$R_{xx}(\tau) = E[x(t)\,x(t+\tau)] = \lim_{T\to\infty}\frac{1}{T}\int_0^T x(t)x(t+\tau)dt \quad , \tag{16}$$

where τ is a time delay between the signal time windows and $E[\cdot]$ represents ensemble-averaging or expected value.

The power spectrum (S_{xx}), or the so-called *auto-spectrum*, is the Fourier transform of the second-order correlation (R_{xx}), which for a discretely sampled data is given by,

$$S_{xx}(f) = \lim_{T\to\infty}\frac{1}{T}E[X(f)\,X^*(f)] \quad , \tag{17}$$

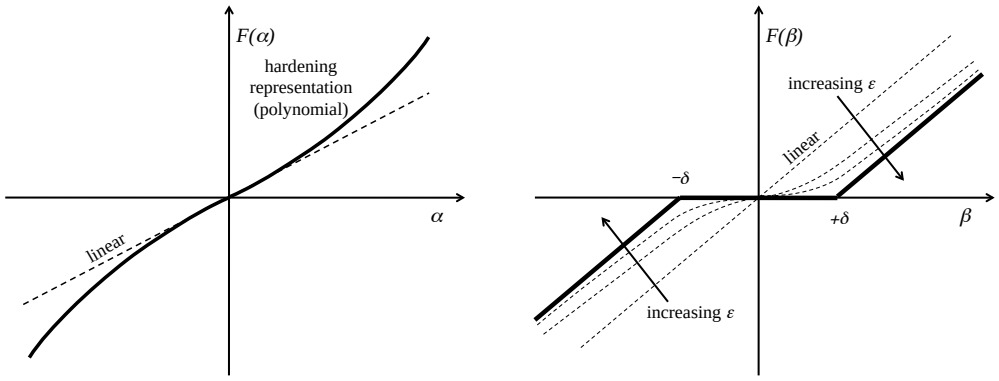

(a) Hardening representation (b) Free-play representation

Figure 3 – Representations for hardening in pitching (rational polynomial approximation) and free-play in control surface deflections (hyperbolic tangent functions combination).

where $X(f)$ is the Fourier transform (amplitude spectrum; *cf.* Eq. (15)) and the superscript (*) denotes complex conjugate.

For a real-valued zero-mean stationary time series, $x(t)$, the higher-order correlation functions, $R_n(\tau_1, ..., \tau_{n-1})$, can be defined as,

$$R_n(\tau_1, ..., \tau_{n-1}) = E[x(t)\ x(t+\tau_1) \cdots\ x(t+\tau_{n-1})]\ . \tag{18}$$

Following Eq. (18), the third- and fourth-order correlation functions, which are referred to as *bicorrelation* and *tricorrelation*, are respectively,

$$R_{xxx} = E[x(t)\ x(t+\tau_1)\ x(t+\tau_2)]\ , \tag{19}$$

$$R_{xxxx} = E[x(t)\ x(t+\tau_1)\ x(t+\tau_2)\ x(t+\tau_3)]\ . \tag{20}$$

The Fourier transform of this moment function gives the third- and fourth-order spectral moments $S_{xxx}(f_1, f_2)$ and $S_{xxxx}(f_1, f_2, f_3)$ that are called *auto-bispectrum* and *auto-trispectrum*, respectively, and given by (similarly as in Eq. (17)),

$$S_{xxx}(f_1, f_2) = \lim_{T\to\infty}(\frac{1}{T})E[X(f_1+f_2)\ X^*(f_1)\ X^*(f_2)]\ \ , \tag{21}$$

$$S_{xxxx}(f_1, f_2, f_3) = \lim_{T\to\infty}(\frac{1}{T})E[X(f_1+f_2+f_3)\ X^*(f_1)\ X^*(f_2)\ X^*(f_3)]\ \ . \tag{22}$$

In nonlinear systems, frequency components can interact to form new components at their sum or difference frequency. When interacting the phase of the new component is related to the phases of the primary interacting modes, therefore by inspecting the phase relation it is possible to identify any nonlinear coupling.

The basis of HOS analysis in detecting nonlinear couplings among frequency modes relies on the fact that if two frequency components (f_1 and f_2) and their sum components (f_1+f_2) are coupled in a time series through a quadratically nonlinear interaction mechanism, phase coherence will exist among them. This arrangement means that a high level of auto-bispectrum is reached. Similarly, the cubic interaction of three frequency components (f_1, f_2 and f_3) yields a large value for the auto-trispectrum.

The auto-bispectrum and auto-trispectrum are usually normalized with respect to the amplitudes of the individual spectral components to yield the *auto-bicoherence* and *auto-tricoherence*. Therefore, based on the Schwartz inequality, are defined respectively as,

$$b^2_{xxx}(f_1, f_2) = \frac{|S_{xxx}(f_1, f_2)|^2}{E[|X_T(f_1+f_2)|^2]E[|X_T(f_1)\ \ X_T(f_2)|^2]}\ \ , \tag{23}$$

$$t^2_{xxxx}(f_1, f_2, f_3) = \frac{|S_{xxxx}(f_1, f_2, f_3)|^2}{E[|X_T(f_1+f_2+f_3)|^2]E[|X_T(f_1)\ \ X_T(f_2)\ \ X_T(f_3)|^2]}\ \ . \tag{24}$$

where $0 < b^2_{xxx}(f_1, f_2) < 1$ and $0 < t^2_{xxxx}(f_1, f_2, f_3) < 1$.

If $b^2_{xxx}(f_1, f_2) = 1$, then the pair of frequency components at f_1 and f_2, as well as their sum f_1+f_2, are quadratically coupled. If $b^2_{xxx}(f_1, f_2) = 0$, frequency components are not coupled, and partially coupled if $0 < b^2_{xxx}(f_1, f_2) < 1$. A two dimensional plot of cut-off planes from auto-bicoherence can reveal regions in which the frequencies are coupled. Similarly, a unit value of auto-tricoherence indicates perfect cubic phase coupling, zero values indicates no coupling, and values between zero and one indicates partial coupling. In this case, to observe the coupling levels it is necessary to plot a three dimensional surface representing a tridimensional cut-off region.

Experimental Model

The experimental apparatus comprises a rigid wing mounted along its span and it is supposed to correlate the bi-dimensional behavior of typical aeroelastic sections. The system allows three degrees of freedom (plunge, pitch, and control surface). The plunge motion is restrained by four elastic steel beams and the pitch stiffness is given by two tension springs connected by a nonlinear cam, which is responsible for the hardening nonlinearity effect. Control surface stiffness is provided by a piano wire and free-play controlled by a pair of adjustable bolts. The measurements of the three degrees of freedom are done using encoders (angular and linear ones). The DSpace® system together with Simulink® are used to signals acquisition and processing. The experimental apparatus is mounted in a open-section wing tunnel ($500 \times 500mm$) (*cf.* Fig. 4 and 5).

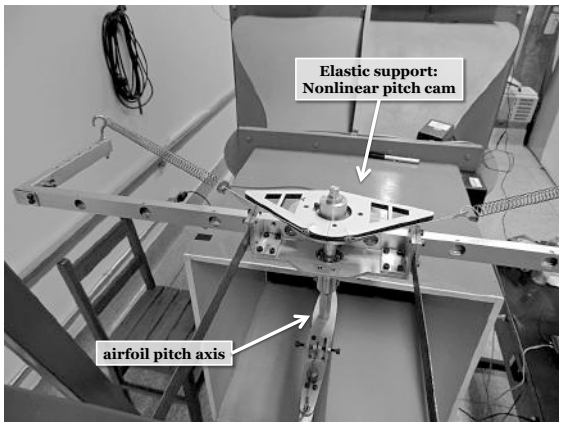

(a) Nonlinear Cam – front view

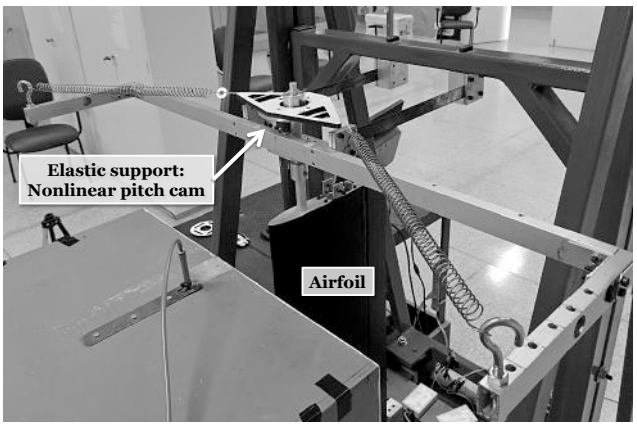

(b) Nonlinear Cam – side view

Figure 4 – Details of the experimental apparatus responsible for the hardening nonlinearity.

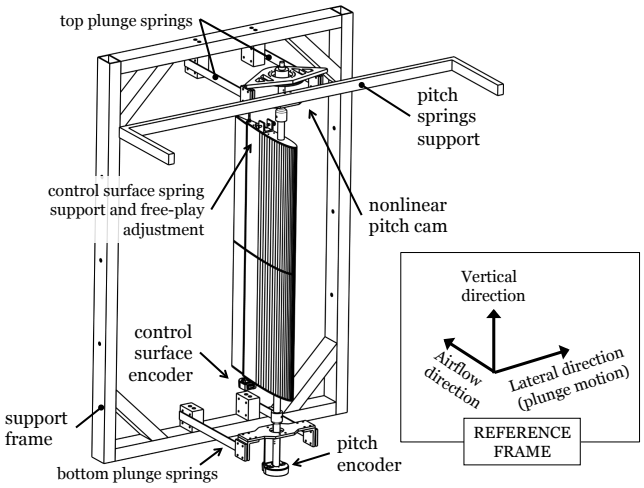

(a) Schematic design of the experimental device

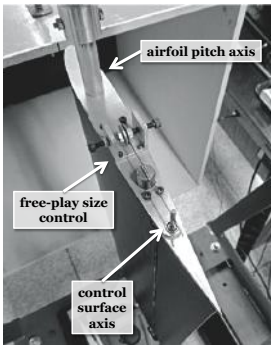

(b) Surface control set-up

Figure 5 – Details of the experimental apparatus and free-play nonlinearity device.

RESULTS

The aeroelastic system is numerically integrated using the Runge-Kutta method. The Table 1 presents the value under consideration in this work.

The three intensities of the hardening nonlinearity in pitching can be obtained by adjusting the pitch spring sizes using the respective support as illustrated in Figs. 4 (a) and (b). The hardening effects vary from large, medium, and small increasing in restoring pitching moment, denoted as hardening 3, 2, and 1 ($cf.$ Fig. 6 (a)), respectively. The restoring moment curve with respect to the pitch angle was assessed and the rational polynomial approximation was used to fit these curves. Table 2 presents the respective RP approximation coefficients for each hardening intensity.

Influence of the hardening nonlinearity

Figures 6 (b), (c) and (d) depict the computational and experimental results of plunging, pitching and control surface motion with no free-play in the control surface for the three different hardening effects considering increasing wind tunnel airflow velocity. The results reveal a smooth subcritical behavior, therefore, the system jumps from his fixed point stability to start LCO with high amplitude before the air velocity reaches the critical flutter speed ($U = U_c$). In the numeric and experiment (in parenthesis) results the LCO amplitude starts in pitch with 2.1° (3.4°), 2.3° (4.4°), and 2.6° (4.8°) for hardenings 3, 2, and 1, when $U = 0.978U_c$ ($U = 0.977{U^*}_c$), respectively.

Table 1 – Experimental values used for the numerical model.

Variables	Specifications	Values
b	Mid-chord (m)	0.125
a	Distance from semichord to elastic axis (nondimensional)	-0.5
c	Hinge line location mesuared from mid-chord (nondimensional)	0.5
ρ	Air density (kg/m^3)	1.078
m_W	Wing mass (kg)	1.5
m_T	Total mass (kg)	4.37
ω_h	Plunge natural frequency (rad/s)	27,32
ω_α	Pitch natural frequency (rad/s)	12,11
ω_β	Flap natural frequency (rad/s)	52.10
x_α	Nondimensional distance between elastic axis and CG of wing	0.66
x_β	Nondimensional distance between hinge line and CG of flap	0.0028
r_α	Nondimensional rotational inertia term about elastic axis	0.7303
r_β	Nondimensional rotational inertia term about hinge line	0.0742
μ	Nondimensional mass ratio	28,34
ζ_h	Plunge modal damping ratio	0,0106
ζ_α	Pitch modal damping ratio	0,3697
ζ_β	Flap modal damping ratio	0,1275
$U_f = U_c$	Linear and critical flutter velocity (Numeric) (m/s)	11,465
U_c^*	Critical flutter velocity (Experiment) (m/s)	$12.10 \leq U_c^* \leq 12.20$

Table 2 – Rational polynomial coefficients for three different intensities of hardening nonlinearities.

	a_3	a_2	a_1	a_0	b_2	b_1	b_0
Hardening 3	7.281	3.01×10^{-2}	1.33×10^{-2}	-1.44×10^{-4}	1.0	6.39×10^{-3}	1.91×10^{-2}
Hardening 2	6.313	-4.58×10^{-2}	3.64×10^{-2}	-2.48×10^{-4}	1.0	-1.06×10^{-2}	2.54×10^{-2}
Hardening 1	6.403	-4.76×10^{-3}	1.26×10^{-1}	-3.03×10^{-4}	1.0	2.61×10^{-7}	6.37×10^{-2}

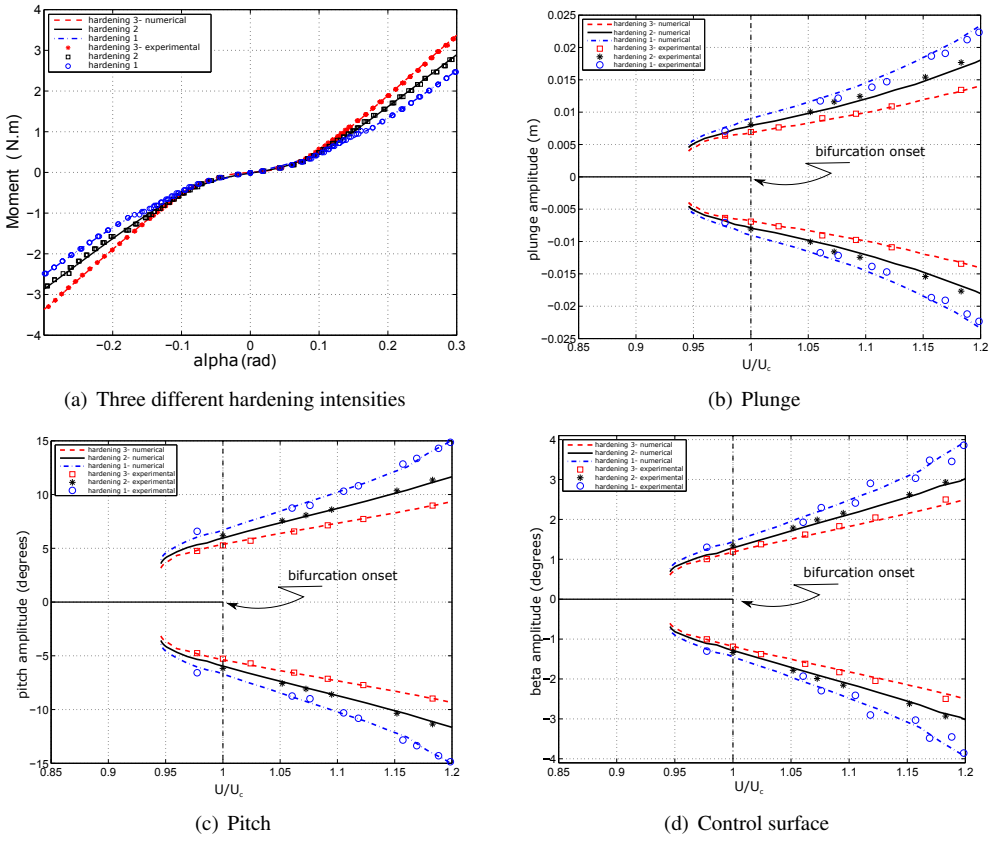

(a) Three different hardening intensities

(b) Plunge

(c) Pitch

(d) Control surface

Figure 6 – Bifurcation diagrams for numerical and experimental results for hardening nonlinearities at different velocities.

Although the hardening nonlinearity has been responsible for the appearance of LCOs, it has not been responsible to changes in supercritical to subcritical behavior, or vice-versa. Moreover, the linear flutter velocity of the system for all LCOs starts and finishes at the same speed. The numerical results have shown good agreement with the experimental

counterparts in which is possible to observe the stronger nonlinearity giving smaller LCO amplitude when the airflow velocity is increased and decreased showing that the hardening can control the amplitude of LCOs.

Influence of the free-play nonlinearity

Admitting hardening 3 nonlinearity in pitching, free-play is included to the control surface hinge. For the analysis different free-play sizes (2δ) were considered, that is, 2° and 4° (*cf.* Fig. 3(b)). Figures 7 (a) and (b) show the computational and experimental results of the surface control LCO amplitudes to increasing of the airspeed, respectively. Subcritical bifurcations can be observed in all cases, but different levels of LCO amplitudes are reveled as the free-play gaps changes. In Figures 7 (a) and (b) the dashed line cases are due to hardening only nonlinearity (that is, $2\delta = 0^\circ$), the solid line cases are due to hardening and free-play ($2\delta = 2^\circ$), and the dash-dot line cases show the subcritical bifurcation for hardening and free-play ($2\delta = 4^\circ$) combination.

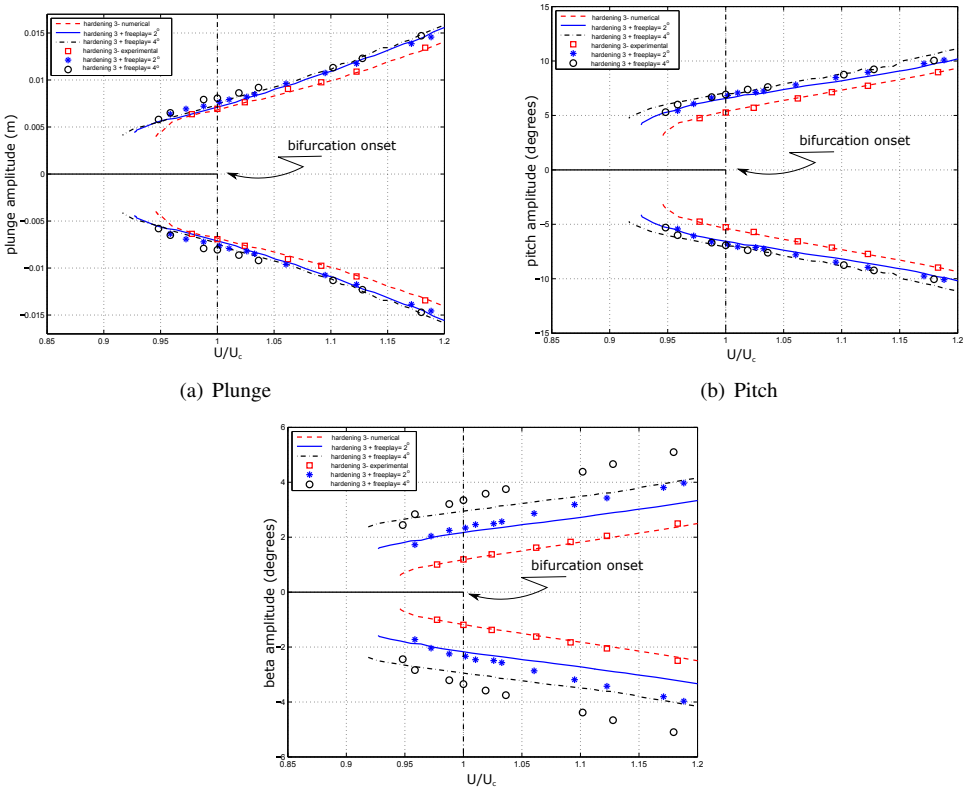

(a) Plunge (b) Pitch

(c) Control surface

Figure 7 – Bifurcation diagrams for numerical and experimental results for free-play nonlinearities combined with hardening 3 nonlinearity in pitching at different velocities.

Here, it is observed that the LCOs for the computational analysis starts in the $U = 0.978U_c$, $U = 0.958U_c$, and $U = 0.938U_c$, respectively, which demonstrates that the subcritical bifurcation also increase as free-play gap size increases. The numerical results are in close agreement with the experimental data, whose results are $U = 0.977U^*{}_c$, $U = 0.958U^*{}_c$ and $U = 0.948U^*{}_c$, respectively.

HOS Analysis

To understand how the nonlinearities are influencing the system and to identify the sources of harmonic couplings, the HOS analysis was applied to the experimental results. The auto-spectrum was used to identify the frequency content of the system, while the auto-bispectrum was used to analyze if there are any quadratic-like nonlinear behavior. Finally, the auto-trispectrum is used to analyze if the system presents cubic-like nonlinear behavior, which is expected since hardening effect was induced to the device thru its nonlinear pitch cam (*cf.* Fig. 4).

Figure 8 presents the power spectrum and the auto-bicoherence contour plot of the pitch motion experimental signals for the system under velocity condition $1.18U_c$. These results consider the system under the hardening 3 nonlinear curve. It is possible to see in the bicoherence contour plot the phase coupling between the fundamental harmonic with itself to generate the first ($2.73Hz$ + $2.73Hz$ = $5.46Hz$) and other super harmonics. It is reasonable to conclude that it is unlikely to build a experimental device without asymmetries. In fact, the apparatus has a small asymmetry in the hardening curves, which can be observed from power spectra (*cf.* Fig. 8 (a) – through the presence of even harmonics).

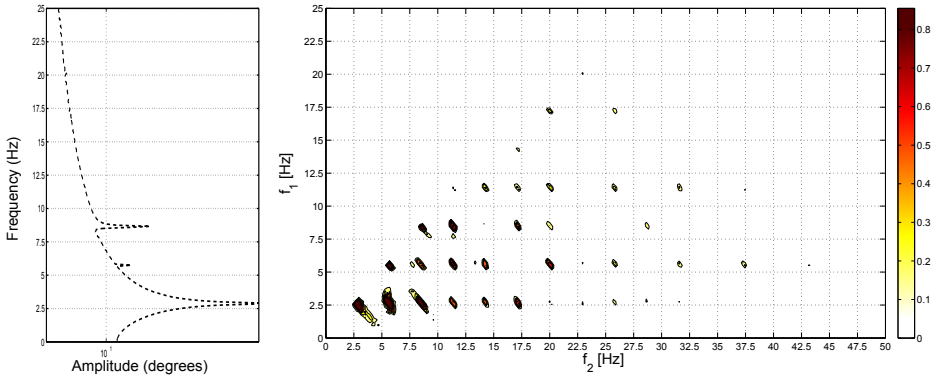

(a) Power spectrum density. (b) Autobicoherence (0 to 1).

Figure 8 – Autobicoherence analysis of the experimental results when the system reaches 1,18$\mathbf{U_c}$ airflow velocity with hardening 3 nonlinearity in the pitch motion.

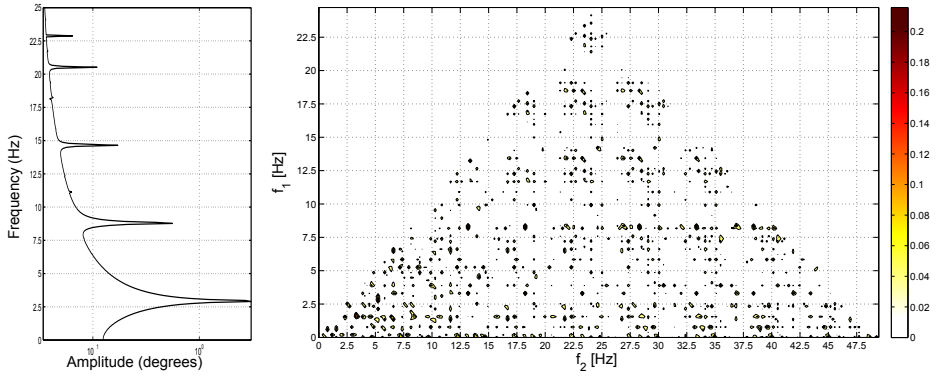

(a) Power spectrum density. (b) Autobicoherence (0 to 1).

Figure 9 – Autobicoherence analysis of the numerical results when the system reaches 1,18$\mathbf{U_c}$ airflow velocity with hardening 3 nonlinearity in the pitch motion without asymmetry (no presence of quadratic coupling).

The auto-bicoherence can be useful to confirm the phase coupling between the fundamental frequency and their even super harmonic frequencies, therefore used to verify typical quadratic-like nonlinear effect. One can conclude from the Fig. 9 that even harmonics comes from the asymmetry since the system does not show the quadratic coupling when the numerical analysis was performed without asymmetry in the hardening curves (*cf.* Fig.9(b)).

Figure 10 (a) and (b) present the auto-tricoherence (contour level is set in 0.8) contour plot and the respective projections for the pitch motion experimental results, when the flow velocity is $1.18U_c$ for the hardening 3 and hardening 1, respectively. There are nonlinear cubic coupling between the fundamental frequency with itself generating the odd super harmonics, which was expected since the system presents hardening nonlinearity in the pitch. It is observed the interaction between the high frequencies increase when the nonlinearity is stronger (*cf.* Figure 10 (a)).

CONCLUDING REMARKS

This paper has presented a study on the influence of structural nonlinearities in a three degrees-of-freedom typical aeroelastic section using the bifurcation analysis. The computational and experimental results have focused on examining the effect of hardening in pitching motion and free-play in the control surface hinge. As observed, the hardening nonlinearity does not change the subcritical or supercritical behavior of the system, but it is responsible for the appearance and amplitude control of LCOs. Otherwise, the free-play leads to the appearance of subcritical behavior and increase the region of dangerous LCO. The results are important to show that nonlinearities can also be good for the dynamics of system in some operational conditions. The HOS analysis has allowed inferring on frequency energy relation between the system dynamics that arises from the nonlinearities. Admitting the experimental apparatus presents a small asymmetry in the hardening curve and a strong cubic nonlinearity behavior, HOS analysis has provided an adequate tool to identify the quadratic and cubic nonlinear effects. As expected the HOS proved to be a great tool for investigation of nonlinear aeroelastic systems.

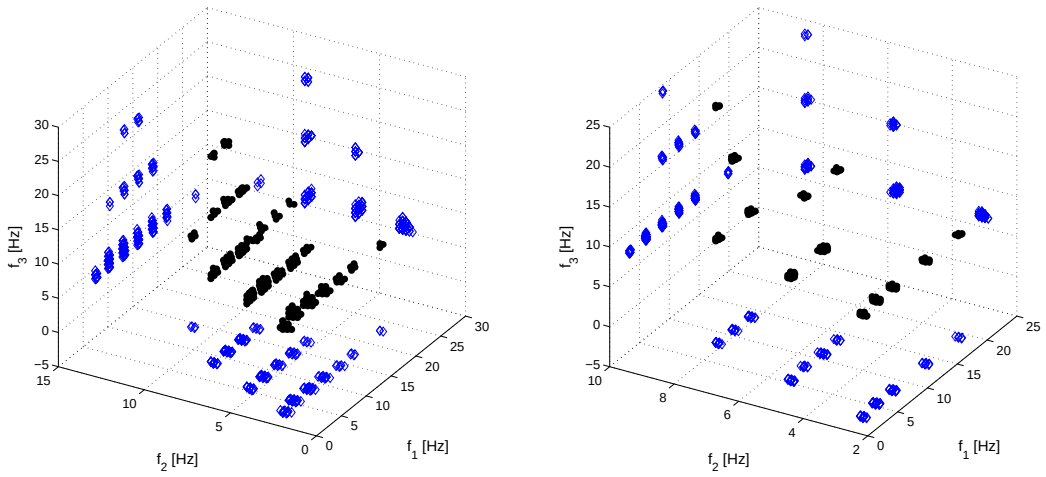

(a) Hardening 3. (b) Hardening 1.

Figure 10 – Autotricoherence of the experimental results when the system reaches 1,18U_c airflow velocity with hardening 3 (a) and hardening 1 (b) in the pitch motion. • - Autotricoherence (cut off= 0,8), ◇- projections.

ACKNOWLEDGMENTS

The authors acknowledge the Coordination for the Improvement of Higher Education Personnel (CAPES) and FAPESP. The authors are also thankful to the Brazilian Research Agencies, CNPq and FAPEMIG, for funding this present research work through the INCT-EIE (National Institute of Science and Technology in Smart Structures in Engineering).

REFERENCES

Bisphinghoff, R.L., Ashley, H. and Halfman, R.L., 1996. Aeroelasticity, Dover Publications.

Chen, P., Sarhaddi, D. and Liu, D., 1998. Limit-cycle-oscillation studies of a fighter with external stores, In Proceedings of the 39^{th} AIAA Structures, Structural Dynamics and Materials Conference, Long Beach, CA. AIAA Paper 98-1727, pp. 258-266.

Dowell, E., Edwards, J., Strganac, T., 2002. Nonlinear Aeroelasticity, Journal of Aircraft, Vol. 40, pp. 857-874.

Hajj, M. R., and Beran, P. S., 2008. Higher-order spectral analysis of limit cycle oscillations of fighter aircraft. Journal of Aircraft, 45(6), 1917-1923.

Lee, B.K.H, Liu, L. and Chung, K.W., 2005. Airfoil motion in subsonic flow with strong cubic nonlinear restoring forces, Journal of Sound and Vibration, Vol. 281, pp. 699-717.

Li, D., Guo, S. and Xiang, J., 2010. Aeroelastic dynamic response and control of an airfoil section with control surface nonlinearities, Journal of Sound and Vibration, Vol. 329, pp. 4756-4771.

Li, D., Guo, S. and Xiang, J., 2012. Study of the conditions that cause chaotic motion in a two-dimensional airfoil with structural nonlinearities in subsonic flow, Journal of Fluids and Structures, Vol. 33, pp. 109-126.

Nayfeh, A.H. and Balachandran, B., 1995. Applied Nonlinear Dynamics: Analytical, Computational and Experimental Methods, Wiley Series in Nonlinear Sciences, John Wiley & Sons, Inc, New York.

O Neill, T., and Strganac, T. W., 1998. Aeroelastic response of a rigid wing supported by nonlinear spring. Journal of Aircraft, 35(4), 616-622.

Sears, W.R., 1940. Operational methods in the theory of airfoils in non-uniform motion, Journal of the Franklin Institute, Vol. 230, pp. 95-111.

Sheta, F., Harrand, V.J., Thompson, D.E. and Strganac, T.W., 2002. Computational and experimental investigation of limit cycle oscillations of nonlinear aeroelastic systems, Journal of Aircraft, Vol. 39, pp. 133-141.

Theodorsen, T., 1935. General theory of aerodynamic instability and the mechanism of flutter, Technical Report 496, NACA Report 496.

Vasconcellos, R.M.G., Abdelkefi, Marques, F.D.and A., Hajj, M. R., 2012. Modeling and analysis of control surface freeplay nonlinearity, Journal of Fluids and Structures, Vol. 31, n.6, pp. 79-91.

Vasconcellos, R.M.G., Abdelkefi, A., Hajj, M. R., Pereira, D.A. and Marques, F.D., 2014. Airfoil control surface discontinuous nonlinearity experimental assessment and numerical model validation, Journal of Vibration and Control.

RESPONSIBILITY NOTICE

The authors are the only responsible for the printed material included in this paper.